

We are IntechOpen, the world's leading publisher of Open Access books Built by scientists, for scientists

6,900

Open access books available

185,000

International authors and editors

200M

Downloads

Our authors are among the

154

Countries delivered to

TOP 1%

most cited scientists

12.2%

Contributors from top 500 universities



WEB OF SCIENCE™

Selection of our books indexed in the Book Citation Index
in Web of Science™ Core Collection (BKCI)

Interested in publishing with us?
Contact book.department@intechopen.com

Numbers displayed above are based on latest data collected.
For more information visit www.intechopen.com



Correlative Light-Electron Microscopy (CLEM) and 3D Volume Imaging of Serial Block-Face Scanning Electron Microscopy (SBF-SEM) of Langerhans Islets

Sei Saitoh

Abstract

Correlative light-electron microscopy (CLEM) is a developing technique for combined analysis of immunostaining for various biological molecules coupled with investigations of ultrastructural features of individual cells within a large field of view. This study first introduces a method of CLEM imaging of the same endocrine cells of compact and diffuse Langerhans islets from human pancreatic tissue specimens. The method utilises serial sections obtained from Epon-embedded specimens fixed with glutaraldehyde and osmium tetroxide. Next, serial block-face imaging using scanning electron microscopy (SBF-SEM) is advanced to enable rapid and efficient acquisition of three-dimensional (3D) ultrastructural information from Langerhans islets of mouse pancreas corresponding to the CLEM images. Samples for SBF-SEM observations were postfixed with osmium and stained en bloc and embedded in conductive resins with ketjenblack significantly reduced the charging of samples during SBF-SEM imaging.

Keywords: correlative light-electron microscopy (CLEM), serial block face SEM (SBF-SEM), compact and diffuse Langerhans islets, conductive resin

1. Introduction

Correlative light-electron microscopy (CLEM) is a developing technique for combined analysis of immunostaining for various biological molecules coupled with investigations of ultrastructural features of individual cells within a large field of view. Combined analysis of immunostaining for various biological molecules coupled with investigations of ultrastructural features of individual cells is a powerful approach for studies of cellular functions in normal and pathological conditions of human Langerhans islets.

Next, serial block-face imaging using scanning electron microscopy (SBF-SEM) is advanced to enable rapid and efficient acquisition of three-dimensional (3D)

ultrastructural information from Langerhans islets of mouse pancreas corresponding to the CLEM images of human. We confirmed the three-dimensional architecture of compact islets (tail) and diffuse islets (head) of the pancreas from normal adult C57BL/6 J mice by SBF-SEM [1].

2. Langerhans islets have compact and diffuse type islets

A large number of endocrine cells, constituting 1–2% of the total volume of the human pancreas in adults, are distributed in more than 1 million islets of Langerhans, first described by Paul Langerhans in 1869. The pancreatic islets, in turn, are distributed throughout the pancreas at variable densities in different lobules, although the density in the tail portion is usually slightly higher [2]. Pancreatic islet endocrine stem cells differentiated to mature islet endocrine cells produce four major peptide hormones: insulin (β -cell granule), glucagon (α -cell granule), somatostatin (δ -cell granule), and pancreatic polypeptide (PP-cell granule), all of which show specific views by electron microscopy [3–5]. Human and rodent pancreases are developed from two different embryological origins; the dorsal origin develops the body and tail portions, whereas the ventral origin derives the head portion of the pancreas. The majority of the pancreas is derived from the dorsal anlage [3, 5–8]. The islets can be classified into two types [5]. “Compact” islets comprise the majority (90%); they are covered by nests of connective tissues. Compact islets are composed of trabeculae of endocrine cells interspersed with clear capsules between adjacent pancreatic exocrine acini [9]. Other islets are “diffuse”; they have no nests separating them from adjacent exocrine acini. However, the ultrastructure supporting “diffuse” pancreatic islets including islet-encapsulating basement membranes, extracellular matrix, and adjacent exocrine acini have not been elucidated in detail [5, 10–13]. Regenerating islet-derived gene 1 alpha (REG1 α) is secreted by the exocrine pancreas or β cells and affects islet cell regeneration [14, 15], thereby regulating the development of Langerhans islet architecture and diabetogenesis [10, 16, 17].

Conventional histochemical methods, such as aldehyde-fuchsin staining, Hellerstrom-Hellman silver staining, and immunohistochemical labelling of peptide hormones, are currently the major approaches used with light microscopy to directly distinguish between types of endocrine cells [18, 19]. Although examination of multiple peptide contents in combination with investigation of the ultrastructural features of individual endocrine cells would provide a detailed analyses of physiological and pathological alterations of pancreatic islets in genetically and epigenetically divergent samples such as human tissues, correlative light and electron microscopy observations combined with double immunostaining using fluorescently labelled secondary antibodies in the same Epon-embedded sample is an improved technique for correlative light-electron microscopy mapping which has been described before [20–24].

3. Correlative light-electron microscopy (CLEM)

For the last quarter century, correlative microscopy, combining the power and advantages of different imaging systems (light, electron, X-ray, NMR, etc.), such as confocal laser scanning microscopy (CLSM), super-resolution microscopy (SFM), transmission electron microscopy (TEM) and scanning electron microscopy (SEM), atomic force microscopy (AFM), magnetic resonance imaging (MRI), superconducting quantum interference devices (SQUIDS), and

in vivo imaging (IVIS[®]) containing micro/nano CT (computed tomography), has become an important tool for biomedical research (**Figure 1**) [25–31]. In particular, the development of a series of hybrid approaches in technological advancements of microscopy techniques, labelling tools, and fixation or preparation procedures allow correlating functional fluorescence microscopy data and ultrastructural information from a singular biological event. A key role in recent advancements of nanotechnology-based biomedical sciences is based on information obtained by light or electron microscopy. As correlative light electron microscopy (CLEM) approaches become increasingly accessible, long-standing questions of biology and clinical medicine regarding structure-function relation are being revisited [26, 31–36].

3.1 Sample preparation for CLEM

3.1.1 Fixation

For good observation of a biological sample in CLEM, fixation remains the ultrastructure of cells or tissue as close to the living material as possible, and subsequent dehydration and embedding. For light microscopy, the chemical fixation was originally designed to preserve the molecular structures of cells and tissues as well as the immunolocalization of components during the subsequent steps of preparation, such as alcohol dehydration and paraffin embedding [37–39]. On the other hand, double fixation with GA and OsSO₄ is suitable for EM observation of the ultrastructure of biomaterials. During the whole process of the fixation and embedding, tissue antigens undergo physicochemical modifications which results in masking of the mostly linear epitopes carried by the tissue components. For that reason, the fixative of immunoelectron microscopy (immuno-EM) is routinely limited to low concentration (0.05~0.5%) glutaraldehyde (GA) and formaldehyde (FA) before antigen-antibody reaction because osmium tetroxide (OsO₄) markedly reduce antigen-antibody response [40, 41].

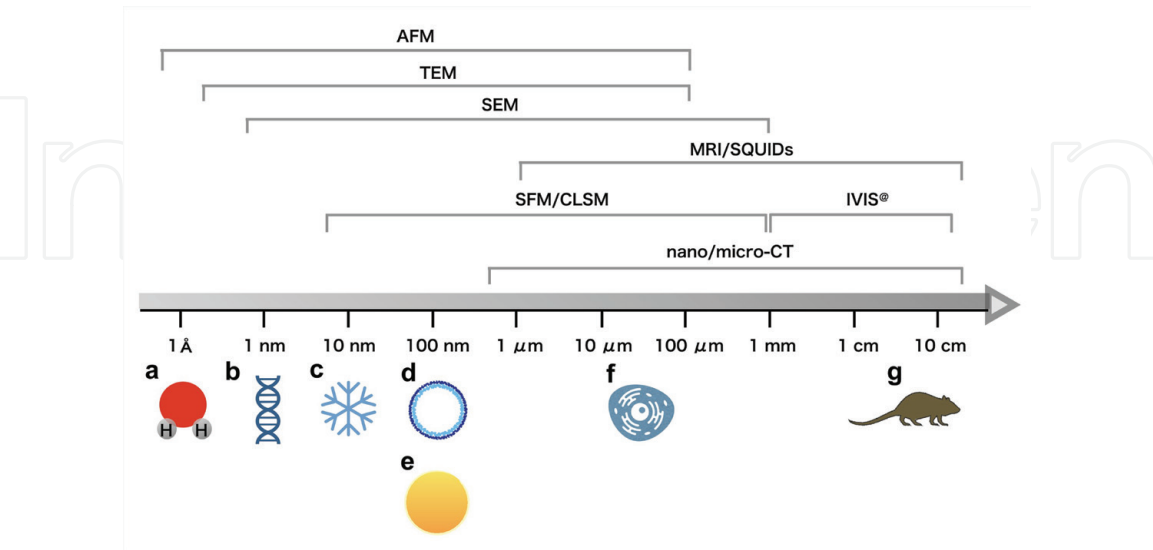


Figure 1. Scale-based representative objects and corresponding microscopic tools for CLEM imaging: atomic force microscopy (AFM), transmission electron microscopy (TEM) and scanning electron microscopy (SEM), magnetic resonance imaging (MRI), superconducting quantum interference devices (SQUIDS), confocal laser scanning microscopy (CLSM), super-resolution microscopy (SFM), and in vivo imaging (IVIS[®]) containing micro/nano CT (computed tomography). (a) H₂O, water molecule (~2 Å), (b) DNA double helix (2–10 nm), (c) dendrimer (1–10 nm), (d) liposome (50–500 nm), (e) gold particle (50–200 nm), (f) cell (5–50 μm), and (g) a mouse (2–10 cm).

3.1.2 Antigen-antibody assay

The quality of correlative image matching critically depends on the ability to maintain the native organisation of cell or tissue during fixation and subsequent sample preparation. Basically, CLEM imaging based on immuno-EM is three different approaches on antigen-antibody assay: (I) serial sectioning, (II) pre-embedding, and (III) post-embedding because TEM imaging is necessary for section-based assay such as ultra-thick sectioning of the embedded samples [26, 35, 42, 43].

I. Serial sectioning

Serial sectioning for CLEM was reported by Baskin D.G et al. (1979), using immunocytochemistry with osmium-fixed tissues, and broadly used for bioscience and clinical medicine embedding in Epoxy resin [20–24, 45].

II. Pre-embedding

In the pre-embedding method, all of the immunostaining is done prior to embedding the tissue. For pre-embedding labelling, all of the immunostaining is done prior to embedding the tissue in resin for ultrathin sectioning on TEM or preparing the samples on SEM. Antigen-antibody reaction is limited by antibody penetration, as usually under 10 μm thickness.

III. Post-embedding

In the post-embedding method, the antigen-antibody reaction is performed on plastic or Tokuyasu cryosections after embedding [46, 47, 99].

3.1.3 Antigen masking

The chemistry of epitope masking itself has been poorly understood. The molecular mechanisms behind antigen masking was that the formaldehyde easily cross-linked amino residues of soluble and structure molecules [48], resulting in artificial changes of the molecular structures.

Antigen masking mechanisms are assumed mainly as follows: (I) molecular modifications of the antigen-carrying proteins upon fixation and embedding, (II) intramolecular modifications leading to antigen masking intrinsic to the protein, and (III) intermolecular effects on other proteins located in close contact with the antigen-bearing one.

3.1.4 Antigen retrieval

To obtain antigen-antibody reaction, some antigen retrieval techniques are frequently used such as enzyme treatment, quick freezing and freeze substitution, freeze-thaw technique, and heating by a microwave apparatus or a high-pressure oven [38, 39, 49–53]. Heat-induced antigen retrieval (HIAR) was developed as a method frequently used for LM and EM samples [49, 51, 53]. The antigen retrieval effect was assumed to be caused by breaks of the cross-linked molecules. Precise mechanisms of (HIAR) is that the extended polypeptides by heating are charged negatively or positively at basic or acidic pH and that an electrostatic repulsion force acts to prevent random entangling of polypeptides caused by hydrophobic attractive force and to expose antigenic determinants,

during cooling process of HIAR solution. HIAR is a powerful tool to all types of immuno-EM for antigen-antibody assay [54–56].

3.2 CLEM using genetically labelled tag

Many biological functions depend critically upon fine details of cell and tissue molecular architecture that developed imaging technique revealing evolutionally. To overcome the limitation of immune assay and capture in vivo imaging and subsequent data acquisition, genetically labelled tag (GFP, mini-SOG, and APEX2) is applied broadly to intact living cells, tissues, and animal models (*Drosophila*, *Caenorhabditis elegans*, zebrafish, and rodents) for 3D CLEM imaging. GFP is converted to HRP-DAB reaction products by photoconversion or by immunolabelling with anti-GFP antibody. New generation of genetically labelled tags (mini-SOG and APEX2) are specialised for CLEM imaging [57–63, 97, 98].

I. Mini singlet oxygen generator (mini-SOG)

Mini-SOG is a small flavoprotein (106 amino acids) derived from *Arabidopsis* phototropin 2 capable of singlet oxygen production upon blue light irradiation to generate the polymerisation of diaminobenzidine into an osmiophilic reaction product resolvable by EM.

II. APEX2

APEX is an engineered peroxidase that functions as an electron microscopy tag and a promiscuous labelling enzyme for live-cell proteomics. APEX2 (enhanced ascorbate peroxidase) is an engineered peroxidase that catalyses DAB reaction to render target structures electron-dense.

3.3 CLEM using formalin-fixed paraffin-embedded sample (FFPE) for clinical medicine

Using haematoxylin and eosin staining or fluorescence immunostaining of paraffin sections of formalin-fixed paraffin-embedded sample (FFPE) for clinical medicine and simple low-vacuum scanning electron microscopy revealed a three-dimensional survey method for assessing cell/tissue architectures. The CLEM methods are applied widely to human biomaterial resources for clinical medicine [64, 65].

3.4 CLEM using glutaraldehyde and osmium tetroxide-fixed Epon-embedded samples for human Langerhans islets

This study is a developing method of correlative light and electron microscopy imaging of the tissue specimens. The method utilises serial sections obtained from Epon-embedded specimens fixed with glutaraldehyde and osmium tetroxide [1].

3.4.1 Tissue preparation

Small pieces of human and mouse pancreatic tissue were prefixed with 2.5% glutaraldehyde in 0.1 M phosphate buffer (PB; pH 7.4) for 1 h and postfixed with 1% osmium tetroxide in 0.1 M PB for 1 h. The specimens were routinely dehydrated by passing the tissue through a series of solutions with increasing ethanol concentrations and then embedded in Epon 812 epoxy resin. To examine the specimens, thick

Epon sections were first cut at 0.5- μm thickness and routinely stained with toluidine blue (TB). These sections were checked and trimmed to visualise Langerhans islets during the next step.

To identify compact and diffuse Langerhans islets, Epon sections of the human pancreas were prepared, routinely fixed with glutaraldehyde and OsO_4 , stained with TB, and observed with a light microscope (**Figure 3**). The compact islets were revealed as large collections of endocrine cells having round to oval shapes (**Figure 3A**, black arrowheads). Their nuclei have homogeneous chromatin patterns with nucleoli, and the cells have moderately light cytoplasm. In contrast, diffuse islets were composed of trabeculae of endocrine cells interspersed between adjacent acini (**Figure 2B**, red arrowheads).

3.4.2 Improved serial sectioning techniques

Then, ultrathin sections were cut at 70–80-nm thickness with a diamond knife on an ultramicrotome and mounted on $\Phi 1 \times 2 \text{ mm}$ single-slit copper grids with a Formvar film covered by evaporated carbon (**Figure 2A**). Then, serial 0.5- μm thick sections were cut and put on MAS-coated glass slides (Matsunami Adhesive Slides, Matsunami Glass, Osaka, Japan) for subsequent immunohistochemical staining (**Figure 2B**).

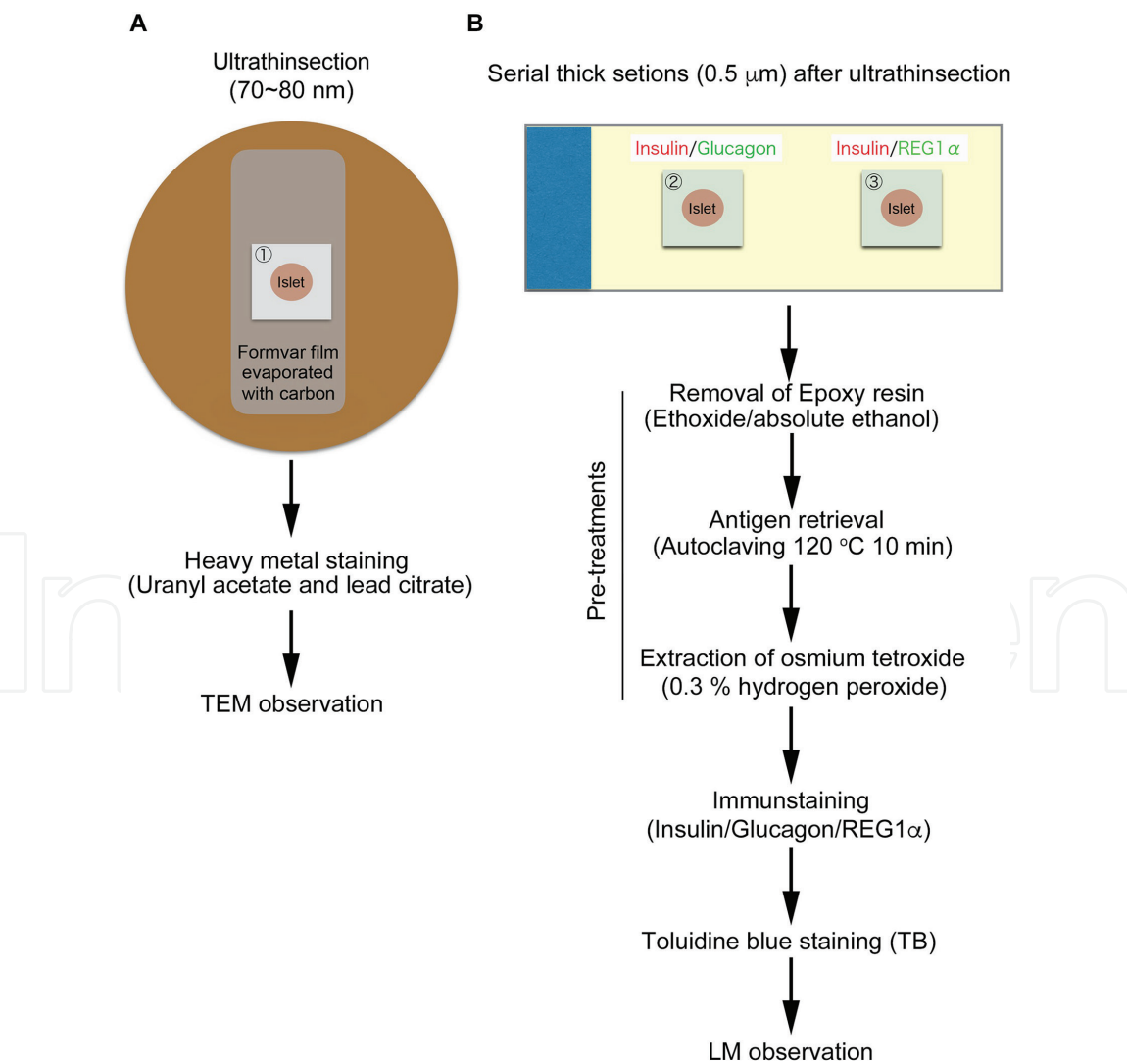


Figure 2. Schematic representation of serial sectioning techniques for correlative light-electron microscopy mapping of human Langerhans islets. A: Schematic images illustrating an ultrathin section of a Langerhans islet mounted on a $\Phi 1 \times 2 \text{ mm}$ single-slit copper grid with a Formvar film covered by evaporated carbon. B: Flow chart of pretreatments and immunohistochemical staining procedures applied to serial thick sections after ultrathin sectioning of Epon blocks.

The ultrathin sections of the human pancreas tissues on copper grids were double-stained with uranyl acetate and lead citrate and, finally, observed under a H-7500 transmission electron microscope (Hitachi, Tokyo, Japan) at an accelerating voltage of 80 kV. Electron microscopy images and montages of Langerhans islets were edited by Photoshop imaging software (Adobe Systems Incorporated, San Jose, CA, USA).

3.4.3 Immunohistochemistry in Epoxy thick sections

Immunohistochemistry in serial thick sections of Epon blocks. The 0.5- μm thick Epon sections on MAS-coated glass slides were placed on a heating plate and heated to 60–80°C for 15 min. During immunohistochemical staining of the peptide hormones (insulin and glucagon) and REG1 α , we noted that two pretreatments after the removal of Epoxy resin, including antigen retrieval by autoclaving and extraction of osmium tetroxide with hydrogen peroxide (**Figure 3**).

3.4.3.1 Pretreatments

I. Removal of Epoxy resin

Epoxy resin was then removed from the sections by treatment with a mixture of ethoxide and absolute ethanol (1,2, v/v) for 30 min, washed in pure ethanol, and rehydrated in phosphate-buffered saline (PBS, pH 7.4). Prior to using the ethoxide/absolute ethanol mixture, saturated sodium ethoxide was aged for approximately 2 weeks until it turned dark brown [20].

II. Antigen retrieval by autoclaving

The specimens underwent two optional pretreatments. For antigen retrieval pretreatment, the specimens were autoclaved in 10 mM sodium citrate buffer (pH 6.0) at 120°C for 10 min and rinsed in PBS.

III. Extraction of osmium tetroxide

To extract osmium tetroxide, the specimens were placed in 0.3% hydrogen peroxide for 10 min and rinsed in PBS.

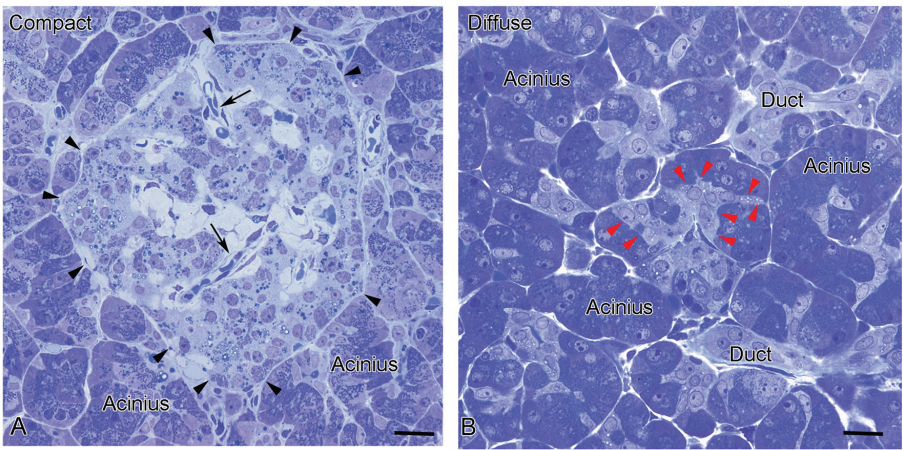


Figure 3. Differences between compact and diffuse islets in human pancreas revealed by light microscopy observations of toluidine blue-stained thick sections routinely embedded in Epon. A: The compact islet appears round to oval and is composed of endocrine cells surrounded with a capsule of connective tissue (black arrowheads). Blood capillaries (black arrows) separate the islet into several lobules. Endocrine cells have moderately light cytoplasm. B: The diffuse islet is composed of a mass of endocrine cells interspersed between adjacent exocrine acinar-like cell clusters without a clear capsule (red arrowheads) in structures that appear like acinar ducts. Bars = 20 μm .

3.4.3.2 Immunoperoxidase-3,3'-diaminobenzidine (DAB) staining

For immunoperoxidase-3,3'-diaminobenzidine (DAB) staining, the specimens were treated with 3% fish gelatin (Sigma-Aldrich, St. Louis, MO, USA) in PBS for 10 min, followed by incubation with each primary antibody (insulin, glucagon, and REG1 α) in PBS at 4°C overnight. Immunoccontrols were performed using the same procedure with the exception that incubation with the primary antibody was omitted. The specimens were then incubated with a horseradish peroxidase (HRP)-conjugated secondary antibody in PBS for 1 h and visualised by exposure to metal-enhanced DAB (Pierce, Rockford, IL, USA) for 5 min. Finally, the specimens were incubated in 0.04% osmium tetroxide in 0.1 M PB for 30 sec to enhance contrast of the DAB reaction products.

The immunoreactivity of the HRP-DAB reaction was dramatically enhanced by autoclave treatment, and the effect was more prominent in insulin immunostaining (**Figure 4D** and **E**, insets; arrows) than in glucagon immunostaining (**Figure 4F** and **G**, insets; arrows). Immunoccontrols not incubated with primary antibodies have reduced backgrounds caused by secondary antibody conjugated-HRP-DAB reaction products and osmification (**Figure 4B** and **C**).

3.4.3.3 Double-fluorescence immunostaining

For single- or double-fluorescence immunostaining experiments, de-osmified thick sections were treated with 3% fish gelatin in PBS for 10 min, followed by primary antibodies in PBS at 4°C overnight. Immunoccontrols were performed using the same procedure with the exception that incubation with the primary antibody was omitted. As secondary fluorescently labelled antibodies, we used Alexa Fluor® 594 and Alexa Fluor 488-conjugated secondary antibodies. Immunostained sections were sealed with VECTASHIELD mounting medium (Vector Laboratories). Fluorescence signals for Alexa Fluor 488 or Alexa Fluor 594 were observed with a BX-61 fluorescence microscope (Olympus, Tokyo, Japan). After obtaining fluorescence images, some thick sections were additionally stained with TB for re-examination of morphology (**Figure 2B**).

Combined analyses using immunohistochemical localisation of hormones and ultrastructure of endocrine cells in animal pituitary glands have been previously reported (Baskin et al., 1979). In those studies, to achieve simultaneous examination, Epon thick sections were prepared from tissues fixed with glutaraldehyde and OsO₄ and peroxidase-DAB immunostaining was used for light microscopy, while electron microscopic observations were carried out in serial ultrathin sections [20]. Conventional double fixation was useful because lipid membranes, such as the plasma membrane of cells and vesicles, are well preserved. Epon-embedded sections are frequently used for ultrastructural analyses by electron microscopy because they exhibit well-preserved tissue morphology. However, the weak tissue antigenicity of Epon-embedded sections poses a problem for immunoassays. There have been attempts to improve immunolabelling of epoxy sections by etching hydrophobic Epoxy resin with different alkali solutions [66], retrieving antigenicity by sodium metaperiodate [21, 67], protease treatments [68], or heating (autoclaving or microwaving) thick or ultrathin sections for immunoelectron microscopy with various salt solutions [45, 56, 69–71]. In the present study, in addition to etching the hydrophobic Epon, we utilised autoclaving and pretreatment with hydrogen peroxide to enhance endocrine peptide immunoreactivity. It is believed that heating treatment retrieves immunoreactivity of masked antigens by exposing epitopes hidden because of cross-linking with aldehyde fixatives, whereas hydrogen peroxide treatment may increase immunoreactivity by reducing osmification of

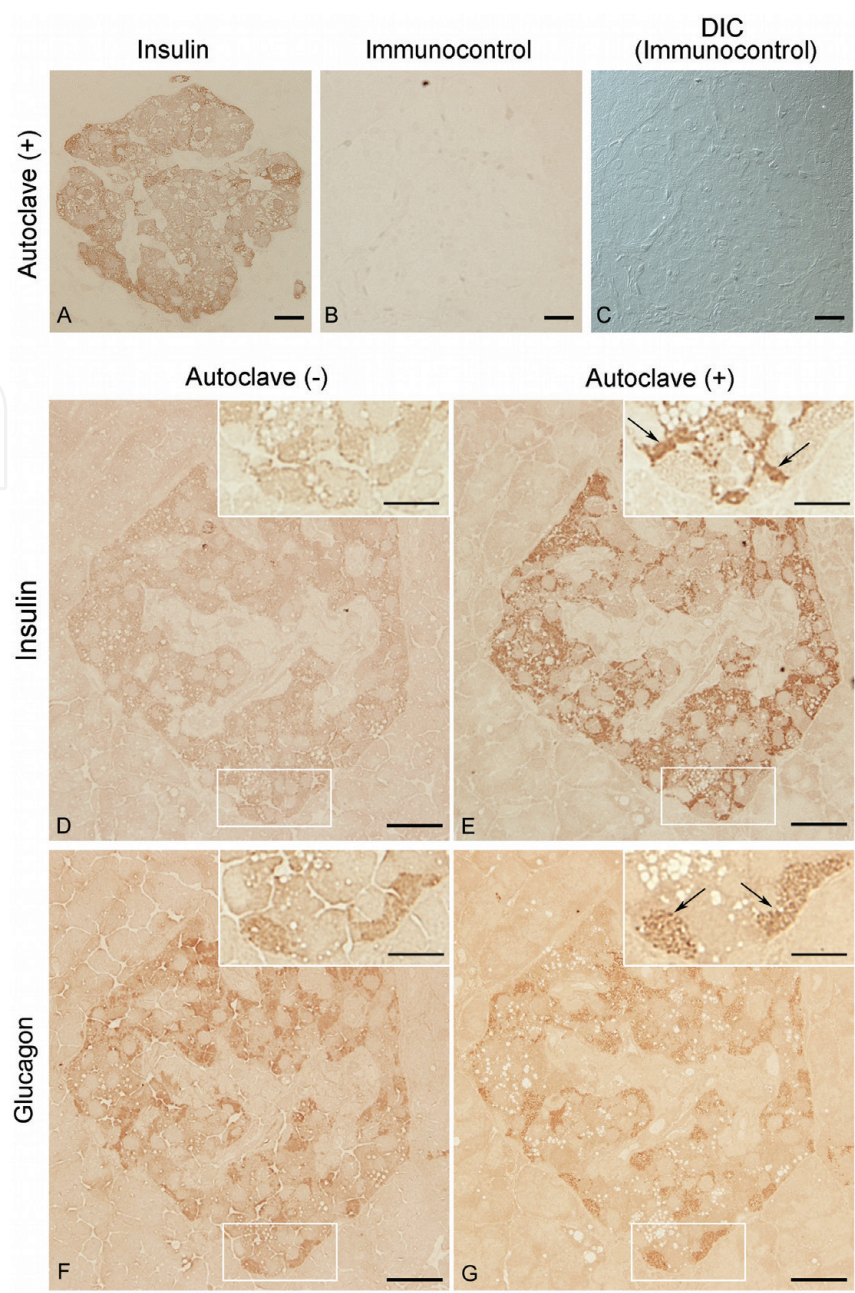


Figure 4. Enhancement of immunostaining for insulin and glucagon in serial thick sections of a typical compact human pancreatic islet by autoclave treatment. A: Insulin-positive staining in a section that underwent autoclave treatment (AC). B: Immunocontrol incubated with secondary antibody without the primary antibody. C: Differential interference contrast microscope (DIC) image of the immunocontrol section. D: Weak insulin immunoreactivity in an untreated section. E: Stronger insulin immunoreactivity in a section that underwent AC—tiny granular patterns are more clearly detected throughout the cytoplasm of β cells (inset, arrows). F: Improved immunoreactivity for glucagon in the cytoplasm of cells in an untreated section. G: Clear granular pattern of immunoreactivity for glucagon in a section that underwent AC (inset, arrows). Bars = 20 μ m (A–G); 10 μ m (D–G, insets).

the target molecules [56, 69]. These pretreatments of Epon section are broadly applied to antibodies of immunohistochemistry not only for peptide hormones but also for several organelle markers: mitochondria, lysosome and peroxisome, or membrane proteins (aquaporin-1, aquaporin-2 and megalin) or soluble proteins—immunoglobulins (IgA and Ig kappa light chain), J chain, and albumin [45, 68, 71]. Overall, we demonstrated that a combination of double fixation, embedding in Epon, and immunohistochemistry with effective pretreatments was a very useful and robust approach for the simultaneous examination of cellular ultrastructure and antigen distribution in individual cells of the human pancreas. Points to be

aware of regarding to pitfall or the limitations of this method: (I) carefully select for combination of first antibodies in double-fluorescence immunostaining, matching for the pretreatment conditions (heating or de-osmification) and (II) weaker DAPI staining for nucleus fluorescence staining after autoclaving [1].

4. CLEM revealed various types of secretory granules in individual endocrine cells of compact and diffuse Langerhans islets of the human pancreas

Correlative light and electron microscopy observations revealed various types of secretory granules in individual endocrine cells of compact and diffuse islets from specimens of the human pancreas (**Figures 5 and 7**).

4.1 Compact type of Langerhans islet

The use of our modified immunostaining protocol allowed clear observations of the ultrastructure of endocrine cells immunopositive for insulin, glucagon, and REG1 α in serial thick and ultrathin sections in compact Langerhans islets of human pancreatic tissue (**Figure 5**). Immunostaining signals for insulin in β -cell granules and for glucagon in α -cell granules did not colocalize in the islet cells (**Figure 5A, D–F**), while patterns of immunostaining for insulin and REG1 α overlapped in large parts of double-immunopositive endocrine cells (**Figure 5G–I**). Immunopositive staining for insulin and glucagon was positive for most islet areas whose ultrastructures were determined in serial ultrathin sections of the same islet (**Figure 5A, D–F, J, and K**). The compact islet illustrated in **Figure 4** had a higher ratio of cells positive for glucagon or insulin compared to cells from the compact islets shown in **Figure 3**. Areas of α or β cells on electron microscopy images were almost completely identical to the areas immunopositive for insulin and glucagon (**Figure 5A, D–F, J, and K**). These correlative observations revealed that islet cells with low and high immunoreactivity for glucagon included round-shaped granules with low and high electron density (**Figure 5P–R**; blue arrows), whereas insulin-positive cells with β -cell granules (**Figure 5O**; red arrows) and condensing vacuoles (**Figure 5O**, white arrows). Immunocontrols that were not incubated with primary antibodies have less background related to the Alexia 488- and Alexia 594-conjugated secondary antibodies and, in particular, because of secondary antibody cross-reactivity to native human immunoglobulins trapped in pancreatic tissues around the blood vessels and fixative autofluorescence.

Some endocrine cells of compact islets exhibited weak immunostaining for glucagon, and two types of round granules—with high and low electron densities—were observed in the same glucagon-positive cells identified in the corresponding areas of serial sections (**Figure 5**). During development and diabetogenesis, α cells may transdifferentiate into β cells for islet regeneration [21, 72]. Granules with a low electron density contain glucagon, glucagon-like peptide (GLP)-1, intervening peptide 2, GLP-2, and preproglucagon which is considered to be undergoing post-translational processing because preproglucagon-containing granules are typically revealed as large α -cell granules with a lower electron intensity [3, 73–75]. In addition, some of the round granules with a low electron density may correspond to δ -cell granules, whose sizes are smaller than those of α -cell granules [76]. We consider that these δ -cell-like granules, which contain somatostatin, would potentially inhibit insulin and glucose secretion, express autocrine or paracrine to somatostatin receptors (SSTRs), and interact with the architecture of the islet [3, 77].

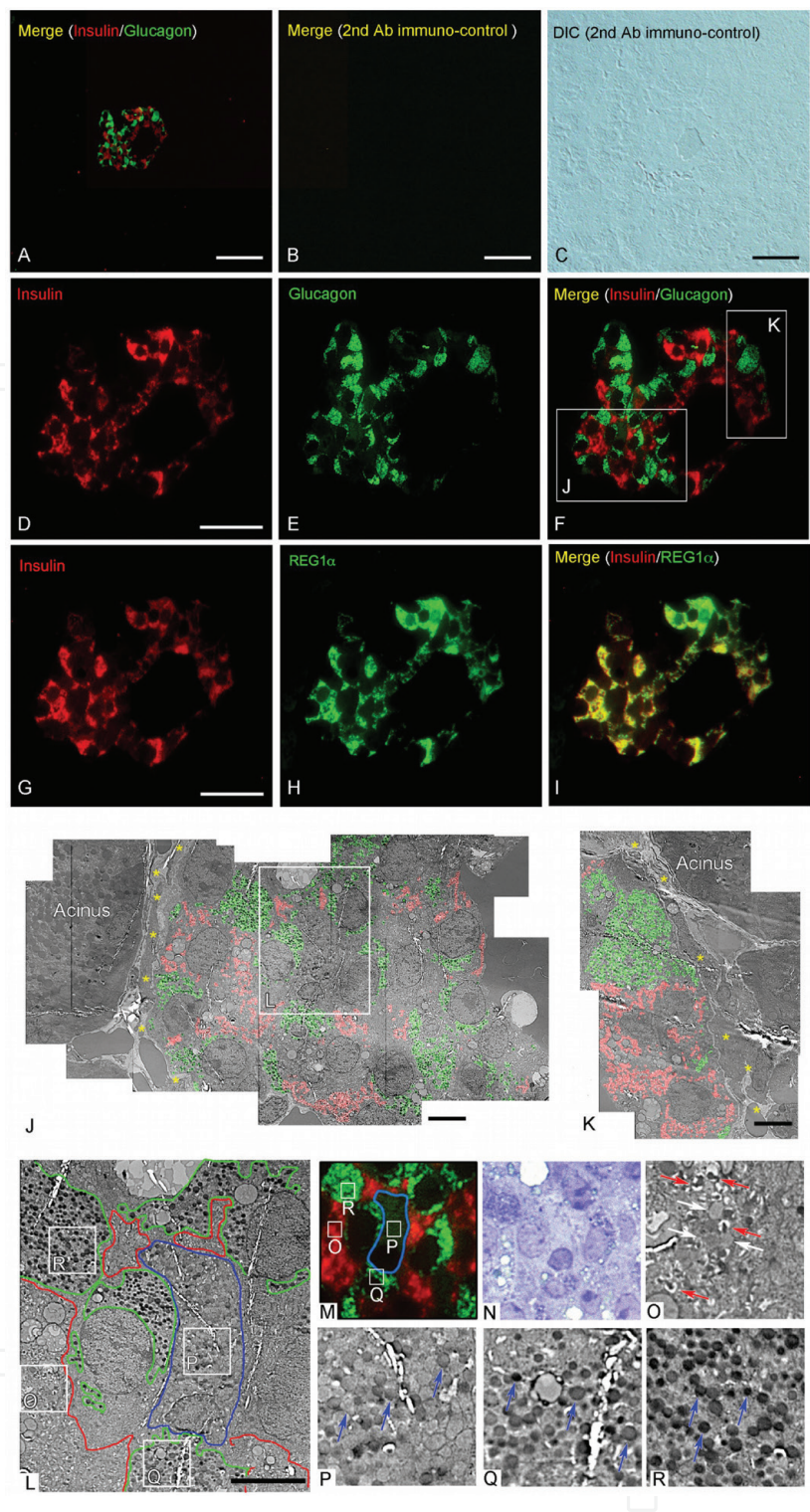


Figure 5. Correlative light-electron microscopy mapping of a compact islet using serial Epon sections from a human pancreatic tissue specimen. Ultrastructural observations and double-immunofluorescence staining for insulin, glucagon, and REG1α were carried out. A: Merged image of insulin- and glucagon-positive staining. B: Merged image of immunocontrol (red and green) exposed to two secondary antibodies without primary antibodies. C: Differential interference contrast microscope (DIC) image of immunocontrol section shown in (B). Islet cells with granular immunopositive staining for insulin (A, D, F, G, I; red) are immunopositive for REG1α (H, I; green), but not for glucagon (A, E, F; green), whereas the immunostaining patterns of insulin and REG1α largely overlap (I; yellow). Electron microscopic montages (J, K) obtained from the same field of the serial section shown in (F). The magnified image (J, K) corresponds to the white boxes in (F). The compact islet has a capsule of connective tissue (J, K; yellow asterisks). Mapping images of β cell granules (J, K; pseudo-coloured red) and α-cell granules (J, K; pseudo-coloured green) manually coloured by Photoshop. Distribution patterns of insulin- (red) and glucagon-positive (green) cells (A, D–F) are clearly identified in the electron micrographs (J, K). Highly magnified electron microscopy images (O–R) correspond to the white boxes in (L) and double-immunopositive staining images (M). N: Toluidine blue staining for the same section (F) of insulin-positive cells (M; red) included β-cell granules (O; red arrows) and condensing vacuoles (O; white arrows), while glucagon-positive cells (M; green) included small numbers of round-shaped granules with low (P; blue arrows), with intermediate (Q; blue arrows) and high (R; blue arrows) electron densities. Bars = 20 μm (A–D, G); 1 μm (J–L).

4.2 Diffuse type of Langerhans islet

Immunoreactive staining for insulin and glucagon was also clearly observed in endocrine cells of diffuse islets, while exocrine cells of adjacent glandular acini were not immunostained (**Figures 6** and **7**). The immunoreactivities for REG1 α and insulin showed different distributions in the same endocrine cells in serial thin sections of diffuse islets (**Figure 5B** and **C**). Fluorescently immunostained sections were subsequently stained with TB, and islet structures were found to be well preserved following double-fluorescence immunostaining (**Figure 7G** and **H**). Electron microscopy observations of serial ultrathin sections were performed to reveal structural details of diffuse islets in addition to identifying the hormones produced by the respective cells (**Figure 7**). It was found that β cells double-positive for REG1 α and insulin were also the cells that exhibited zymogen-like condensing vacuoles (200–500 nm in size) and many organelles, such as mitochondria, Golgi apparatus, endoplasmic reticulum (ER), and lipofuscin granules (**Figure 7J** and **L**, white arrows) [78]. In addition, these endocrine cell granules in contact with exocrine acinar-like cell clusters have electron-dense cores and clear halos. However, insulin and REG1 α double-positive endocrine cells consisted of several granular morphologies of human islet endocrine cells. We classified the granules of human islets into four types (α -, β -, δ -, and PP-cell granules) as described previously [3, 5, 74, 76] where (I) α -cell type (glucagon secretory), electron-dense without a clear halo occasionally presenting with a grey halo (**Figure 6K**, red arrowheads); (II) β -cell type (insulin secretory), granules of this type have electron-dense cores with a crystalline shape (**Figure 7K–N**, blue arrowheads); (III) δ -cell type (somatostatin secretory), larger and electron-opaque (**Figure 7K, L**, and **N**, cyan arrowheads); and (IV) PP-secretory cell type, spherical and smaller granules with a small halo (**Figure 7L**, green arrowheads). Interestingly, islet endocrine cells in contact with adjacent exocrine acinar-like cell clusters (ATLANTIS) contained zymogen-like granules (**Figure 7M**, yellow arrow), and cell-to-cell contacts were also detected (**Figure 7N**, white arrows).

Correlative light and electron microscopy analyses of serial thick and ultrathin sections showed intracellular organelles and membrane interdigitations near cell-to-cell contact areas as well as typical α - or β -cell granules in individual insulin- and glucagon-positive endocrine cells located in both compact and diffuse islets (**Figures 5** and **7**). Human Langerhans islets contain polygonal endocrine cells that are demarcated by intercellular structures, such as tight junctions, gap junctions, and membrane structures, including interdigitations and invaginations [44]. In diffuse Langerhans islets, we found that some endocrine cells appear to

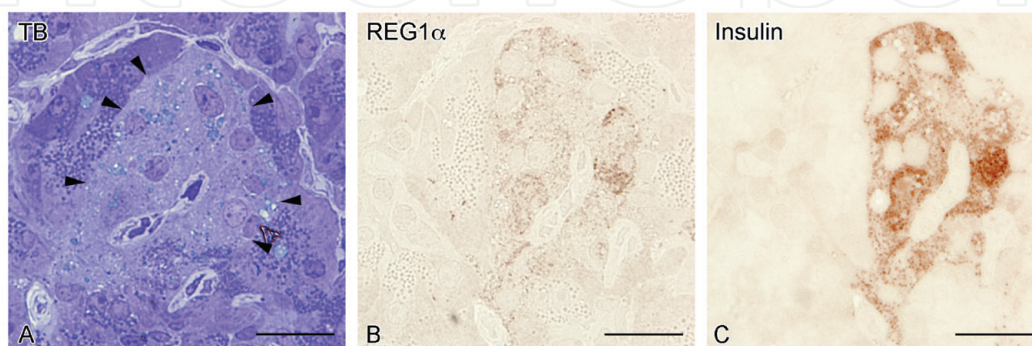


Figure 6. Different distributions of HRP-DAB-immunoreaction products for REG1 α and insulin in the same endocrine cells of diffuse type islet in serial thick sections of a diffuse human pancreatic islet. The diffuse islet is composed of a mass of endocrine cells interspersed between adjacent exocrine acinar-like cell clusters without a clear capsule (A; arrowheads). Islet endocrine cells show granular immunopositive staining for REG1 α (B) or insulin (C), while acinar-like cells in contact with islet endocrine cells were not immunostained. TB: toluidine blue staining. Bars = 20 μ m.

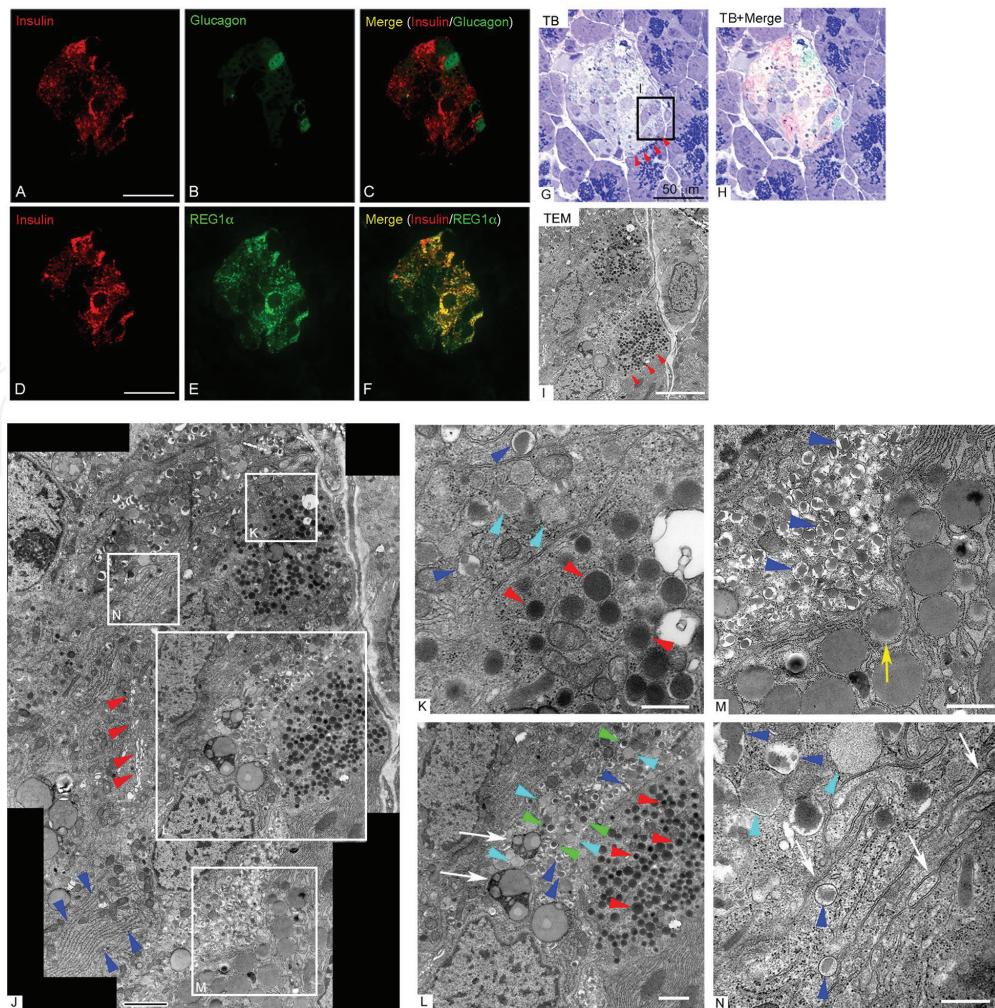


Figure 7. Correlative light-electron microscopy mapping of a diffuse islet using serial Epon sections from a human pancreatic tissue specimen. Ultrastructural observation and double-immunofluorescence staining for insulin, glucagon, and REG1 α were carried out. Granular immunoreactivities for insulin (A, C; red) and glucagon (B, C; green) are sparse and dense respectively, while the immunostaining patterns of insulin (D, F; red) and REG1 α (E, F; green) largely overlap. G: A light microscopy image of the same thick section stained with toluidine blue (TB) after microscopy observation of fluorescence immunostaining (A–C). The diffuse islet is composed of a mass of endocrine cells in contact with adjacent exocrine acinar-like cell clusters without a clear capsule (red arrowheads). H: Superimposed image of (C) and (G). I: An electron microscopy image of the black-boxed area shown in (G) obtained from a serial ultrathin section demonstrating the ultrastructural features of insulin- and glucagon-positive endocrine cells in a diffuse pancreatic islet. The diffuse islet is composed of a mass of endocrine cells interspersed between exocrine acinar-like cell clusters without a clear capsule (red arrowheads). J: An electron microscopy montage showing a pancreatic islet corresponding to the rectangle of TB staining shown in (G). Endoplasmic reticulum and Golgi apparatus are indicated by blue and red arrowheads, respectively. K: A higher-magnification image of the respective boxed area in (J) illustrating an α cell containing α -cell granules (red arrowheads) in contact with a β cell containing β -cell granules (blue arrowheads) and condensing small vacuoles (cyan arrowheads). L: A higher-magnification image of the respective boxed area in (J) illustrating a β cell with β -cell granules (blue arrowheads) and spherical and smaller granules with small halo (green arrowheads) in contact with an α cell containing α -cell granules (red arrowheads). M: A higher-magnification image of the respective boxed area in (J) illustrating a β cell with β -cell granules (blue arrowheads) and a zymogen-like granule (yellow arrow) in cell-to-cell contact with an exocrine acinar-like cell containing zymogen-like granules. N: Interdigitation of cell membranes (white arrows) containing β -cell granules (blue arrowheads) and 200–500-nm condensing vacuoles (cyan arrowheads) between two β cells. Bars = 50 μ m (A, D, G); 5 μ m (I); 2 μ m (J); 500 nm (K, N); 1 μ m (L, M).

have direct cell-to-cell contacts with adjacent endocrine and exocrine acinar-like cells (**Figure 7**). These results indicate that electric or metabolic coupling exists not only between adjacent endocrine cells but also between endocrine cells and the surrounding pancreatic exocrine acinar-like cell clusters [10, 44]. We also identified insulin and REG1 α double-positive cells that contained zymogen-like condensing granules in the endocrine islet cells, with several types of granules morphologically classified as β -, δ -, and PP-cell like granules (**Figure 6**).

5. Three-dimensional scanning electron microscopy (3D SEM) with volume imaging

Scanning electron microscopy (SEM) is a powerful technique for three dimensional CLEM imaging. SEM is traditionally used for imaging detecting the surface of cells, tissues, and the whole multicellular organisms by secondary electron beam. Recently, the critical advancement includes serial ultrastructural observation with scanning electron microscopy (SEM) using backscattered electron with specific tissue preparation methods to increase heavy metal deposition for efficient SEM imaging. In brief, three volume SEM methods: serial block-face electron microscopy (SBF-SEM), focused ion beam SEM (FIB-SEM), and array tomography using serial sectioning are illustrated in **Figure 8** [79–85, 96].

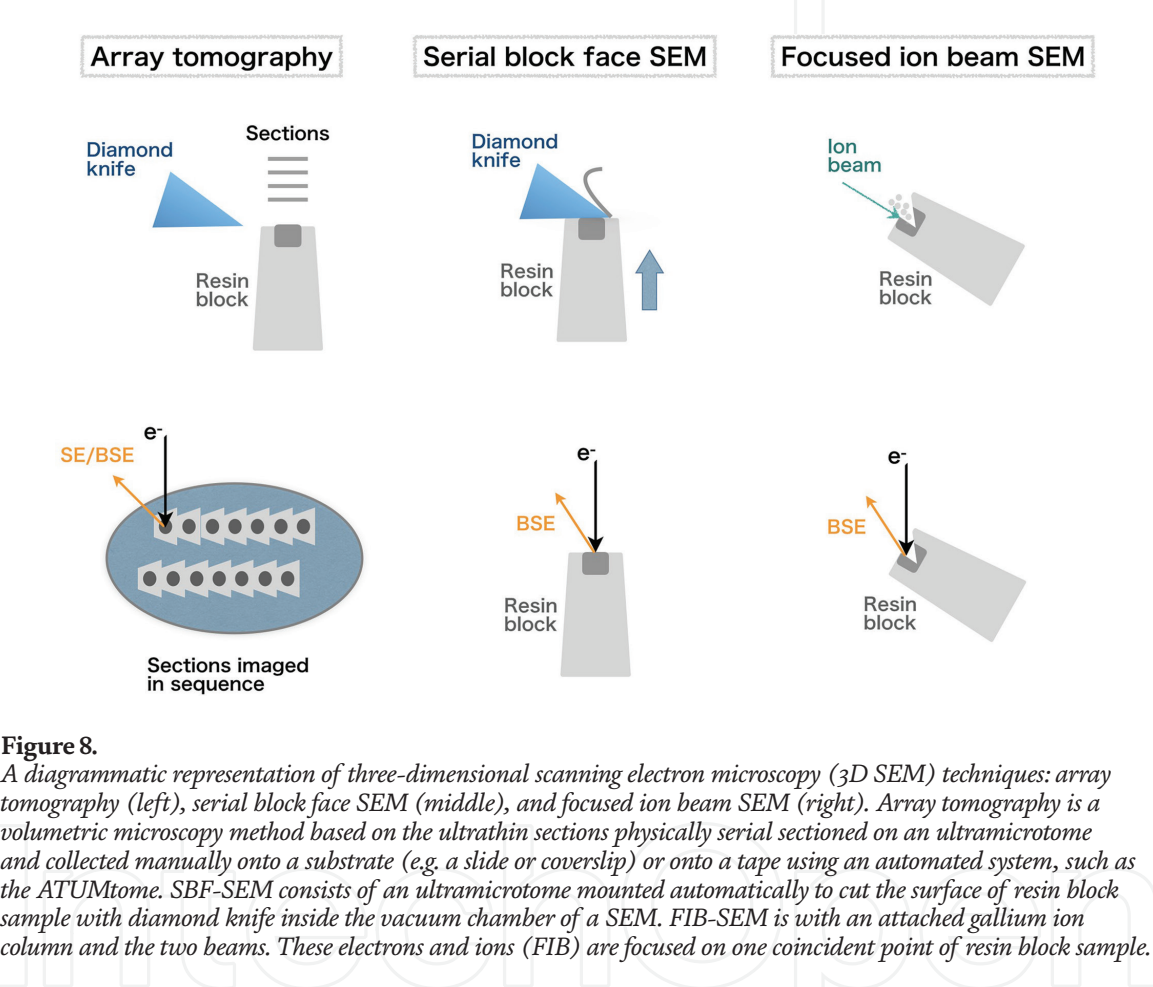


Figure 8. A diagrammatic representation of three-dimensional scanning electron microscopy (3D SEM) techniques: array tomography (left), serial block face SEM (middle), and focused ion beam SEM (right). Array tomography is a volumetric microscopy method based on the ultrathin sections physically serial sectioned on an ultramicrotome and collected manually onto a substrate (e.g. a slide or coverslip) or onto a tape using an automated system, such as the ATUMtome. SBF-SEM consists of an ultramicrotome mounted automatically to cut the surface of resin block sample with diamond knife inside the vacuum chamber of a SEM. FIB-SEM is with an attached gallium ion column and the two beams. These electrons and ions (FIB) are focused on one coincident point of resin block sample.

6. Serial block-face scanning electron microscopy (SBF-SEM) revealed novel architecture of Langerhans islets

Serial block-face imaging using scanning electron microscopy (SBF-SEM) is advanced to enable rapid and efficient acquisition of three-dimensional (3D) ultrastructural information of large field of 3D volume imaging such as Langerhans islet over 100 μm size, providing a highly spatial resolution of the ultrastructure of diffuse islets from the head portion of mouse pancreas, which has a ventral origin [8, 86, 87].

6.1 Sample preparation using conductive Epon with carbon (ketjenblack)

Samples for SBF-SEM observations were postfixed with osmium and stained en bloc, as described previously. Briefly, mouse pancreatic tissues were prefixed with

2.5% glutaraldehyde in 0.1 M phosphate buffer (PB; pH 7.4) overnight, and tissues were washed with cacodylate buffer (pH 7.4). Notice that perfusion-fixation is easy to open the vessels and cell-to-cell contacts due to pressure artefacts. Tissues were then treated with 2% OsO₄ (Nisshin EM, Tokyo, Japan) in 0.1 M cacodylate buffer containing 0.15% K₄[Fe(CN)₆] (Nacalai Tesque, Kyoto, Japan) for 1 h on ice and 0.1% thiocarbohydrazide (Sigma-Aldrich) for 20 min and 2% OsO₄ for 30 min at room temperature. Thereafter, the tissues were treated with 2% uranyl acetate at 37°C for 3 h. Tissues were then treated with lead aspartate solution at 60°C for 30 min. The specimens were routinely dehydrated by passing the tissue through a series of solutions with increasing ethanol concentrations; infiltrated with acetone dehydrated with a molecular sieve, a 1:1 mixture of resin and acetone, and 100% resin; and then embedded in Epon 812 epoxy resin with carbon (ketjenblack) at 60°C for 3 days/overnight. Epon 812 epoxy resin with/without carbon (ketjenblack) enables for three-dimensional (3D) ultrastructural information of a large field of 3D volume imaging such as Langerhans islet over 100 µm size. Following trimming of islets from mouse pancreas, samples were imaged with a SigmaTMVP (Carl Zeiss, Munich, Germany) equipped with 3View (Gatan Inc., Pleasanton, CA, USA). The serial images of SBF-SEM were handled with Fiji/ImageJ and segmented and reconstructed to 3D images using MIB (<http://mib.helsinki.fi/>) and Amira software.

Samples for SBF-SEM observations were postfixed with osmium and stained en bloc and embedded in conductive resins with ketjenblack significantly reduced the charging of samples during SBF-SEM imaging. Conductive resins were produced by adding the carbon black filler, ketjenblack, to resins commonly used for electron microscopic observations of biological specimens. Carbon black mostly localised around tissues and did not penetrate cells, whereas the conductive resins significantly reduced the charging of samples during SBF-SEM imaging. When serial images were acquired, embedding into the conductive resins improved the resolution of images by facilitating the successful cutting of samples in SBF-SEM [1, 88].

6.2 ATLANTIS in diffuse type of Langerhans islet

Endocrine cells from diffuse islets were also in contact with adjacent exocrine acinar-like cell clusters (ATLANTIS) without a clear capsule (**Figure 8D–I**). The morphologies of granules in endocrine cells of diffuse islets (**Figure 8F**) mainly consisted of three types: (I) granules with a spherical dense core and a small halo similar to PP-cell granules (**Figure 9F**, green arrowheads), (II) granules with a low electron-dense core without halo similar to δ -cell granules (**Figure 8F**, cyan arrowheads), and (III) granules with a spherical or crystal-shaped dense core with a clear halo similar to β -cell granules [87].

Serial SBF-SEM images revealed that zymogen-like granules are broadly distributed in these endocrine islet cells in contact with acinar-like cells. The zymogen-like granules have an isotropic distribution from ATLANTIS to the islet cells through direct contact with lamellar ERs in diffuse islets of the pancreatic head portion in adult normal mice derived from ventral origins (**Figure 9G–I**). Electron microscopic observations showed the same architecture in human diffuse islets in contact with acinar-like cells without a clear capsule. The typical diffuse endocrine islet in contact with acinar-like cells showed typical features of being rich in PP with a paucity of glucagon [3, 8]. Further, endocrine islet cells colocalised most of the PP-cell-like granules and zymogen-like granules directly through cell-to-cell contact sites with lamellar ERs, even if zymogen-like granules were excreted from the ATLANTIS. Using the correlative light and electron microscopy imaging described in the present study, additional basic and clinical studies for the precise

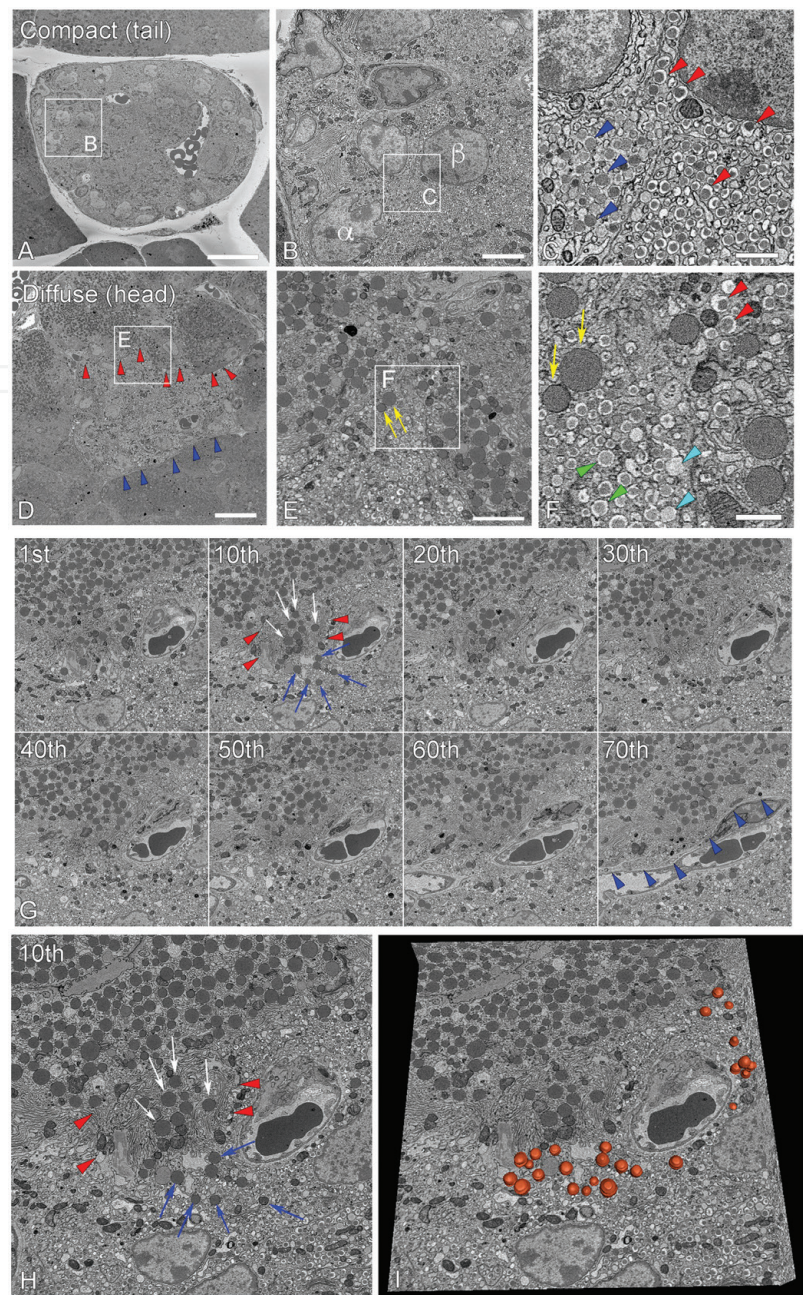


Figure 9. Serial block-face scanning electron microscopy (SBF-SEM) observations of compact and diffuse islets from pancreatic tissues of a C57BL/6 J mouse. A: The compact islet is composed of a mass of endocrine cells with a clear capsule from the tail portion of the pancreas. B: α cells and β cells localised in the corner of an islet in contact with a capsule. C: α -cell granules (blue arrowheads) are electron-dense without a core, while β -cell granules (red arrowheads) show angular-shaped cores with a clear halo. D–E: The diffuse islet is composed of a mass of endocrine cells in contact with adjacent exocrine acinar-like cell clusters (ATLANTIS) (red arrowheads) without a clear capsule (blue arrowheads). F: The islet endocrine cells contain three type of granules: (1) spherical smaller granules with a small halo (green arrowheads), (2) slightly electron-opaque but spherical granules without a halo having a similar size to α -cell granules (cyan arrowheads), and (3) granules with zymogen-like granules (yellow arrows). The ATLANTIS containing β -cell granules (red arrowheads). G: Montage picture of the islet endocrine cells and ATLANTIS in the diffuse islet (D) showing every 10 serial images of a total of 70 images at 50-nm thickness each. The ATLANTIS containing zymogen-like granules (G10th, white arrows), isotopically localised to the islet cells (G10th, blue arrows), and in direct contact with endocrine cells with lamellar endoplasmic reticuli (G10th, red arrowheads). Islet cells are partially separated from the acinar-like cell clusters with connective tissues by blood vessels (G70th, blue arrowheads). H: Magnified image of (G10th). I: Three-dimensional reconstruction of serial images indicating the zymogen-like granules (shown in orange) inside the islet endocrine cells in contact with ATLANTIS.

identification of the observed granules in glucagon- and insulin-positive cells as well as the immunohistochemical detection of peptide components in human Langerhans islets for detailed clinical analyses of diabetes mellitus and chronic

kidney or intestinal diseases closely related to metabolic disorders warrant further investigation [4, 5, 10, 16, 71, 78, 79, 89–93].

Interestingly, recently developed super-resolution microscopy (SRM) enables a detailed analysis distribution of biological molecules at an even higher resolution (e.g. a lateral resolution of 20–50 nm) by stochastic optical reconstruction microscopy when it is combined with new light microscopy technologies for nano-level analyses, an approach which may be applied to chemically fixed and Epon-embedded specimens [30, 33, 94, 95]. In combination with immunohistochemistry and in situ hybridization in Epon sections, the correlative microscopy observation method would be a more powerful approach capable of revealing human islet regeneration under genomic and transcriptome control such as SSTR expression in β cells from human islets [3, 70, 77].

Acknowledgements

This work was supported by the JSPS KAKENHI Grant Number 16 K08439 and by the EM facility in the National Institute for Physiological Sciences in Japan.

Competing interest statement

The authors declare that there are no conflicts of interest.


Author details

Sei Saitoh

Department of Anatomy II and Cell Biology, Fujita Health University School of Medicine, Toyoake, Japan

*Address all correspondence to: saitoh@fujita-hu.ac.jp

IntechOpen

© 2018 The Author(s). Licensee IntechOpen. This chapter is distributed under the terms of the Creative Commons Attribution License (<http://creativecommons.org/licenses/by/3.0>), which permits unrestricted use, distribution, and reproduction in any medium, provided the original work is properly cited. 

References

- [1] Saitoh S, Ohno N, Saitoh Y, Terada N, Shimo S, Aida K, et al. Improved serial sectioning techniques for correlative light-electron microscopy mapping of human Langerhans islets. *Acta Histochemica et Cytochemica*. 2018;**51**:9-20
- [2] Wittingen J, Frey CF. Islet concentration in the head, body, tail and uncinate process of the pancreas. *Annals of Surgery*. 1974;**179**:412-414
- [3] Brereton MF, Vergari E, Zhang Q, Clark A. Alpha-, delta- and PP-cells: Are they the architectural cornerstones of islet structure and co-ordination? *The Journal of Histochemistry and Cytochemistry*. 2015;**63**:575-591
- [4] Briant L, Salehi A, Vergari E, Zhang Q, Rorsman P. Glucagon secretion from pancreatic α -cells. *Upsala Journal of Medical Sciences*. 2016;**121**:113-119
- [5] Mills SE. *Histology for Pathologists*. 4th ed. Philadelphia: Wolters Kluwer Health/Lippincott Williams & Wilkins; 2012. pp. 777-816
- [6] Kaung HC. Glucagon and pancreatic polypeptide immunoreactivities co-exist in a population of rat islet cells. *Experientia*. 1985;**41**:86-88
- [7] Oikawa T, Ogawa K, Taniguchi K. Immunocytochemical studies on the pancreatic endocrine cells in the Japanese newt (*Cynopus pyrrhogaster*). *Experimental Animals*. 1992;**41**:505-514
- [8] Suda K, Mizuguchi K, Hoshino A. Differences of the ventral and dorsal anlagen of pancreas after fusion. *Acta Pathologica Japonica*. 1981;**31**:583-599
- [9] Grube D, Bohn R. The microanatomy of human islets of Langerhans, with special reference to somatostatin (D-) cells. *Archivum Histologicum Japonicum*. 1983;**46**:327-353
- [10] Aida K, Saitoh S, Nishida Y, Yokota S, Ohno S, Mao X, et al. Distinct cell clusters touching islet cells induce islet cell replication in association with over-expression of Regenerating Gene (REG) protein in fulminant type 1 diabetes. *PLoS One*. 2014;**9**:e95110
- [11] Bensley RR. Studies on the pancreas of the guinea pig. *The American Journal of Anatomy*. 1911;**12**:297-388
- [12] Bonner-Weir S, Smith FE. Islets of Langerhans: Morphology and its implications. In: Kahn CR, Weir GC, editors. *Joslin's Diabetes Mellitus*. 13th ed. Philadelphia: Lea & Febiger; 1994. pp. 15-28
- [13] Dewitt LM. Morphology and physiology of areas of Langerhans in some vertebrates. *The Journal of Experimental Medicine*. 1906;**8**:193-239
- [14] Terazono K, Uchiyama Y, Ide M, Watanabe T, Yonekura H, Yamamoto H, et al. Expression of reg protein in rat regenerating islets and its co-localization with insulin in the beta cell secretory granules. *Diabetologia*. 1990;**33**:250-252
- [15] Watanabe T, Yonekura H, Terazono K, Yamamoto H, Okamoto H. Complete nucleotide sequence of human reg gene and its expression in normal and tumoral tissues. The reg protein, pancreatic stone protein, and pancreatic thread protein are one and the same product of the gene. *The Journal of Biological Chemistry*. 1990;**265**:7432-7439
- [16] Calderari S, Irminger JC, Giroix MH, Ehse JA, Gangnerau MN, Coulaud J, et al. Regenerating 1 and 3b gene expression in the pancreas of type 2 diabetic Goto-Kakizaki (GK) rats. *PLoS One*. 2014;**9**:e90045
- [17] Xu W, Li W, Wang Y, Zha M, Yao H, Jones PM, et al. Regenerating

islet-derived protein 1 inhibits the activation of islet stellate cells isolated from diabetic mice. *Oncotarget*. 2015;**6**:37054-37065

[18] Brissova M, Fowler MJ, Nicholson WE, Chu A, Hirshberg B, Harlan DM, et al. Assessment of human pancreatic islet architecture and composition by laser scanning confocal microscopy. *The Journal of Histochemistry and Cytochemistry*. 2005;**53**:1087-1097

[19] Lumelsky N, Blondel O, Laeng P, Velasco I, Ravin R, McKay R. Differentiation of embryonic stem cells to insulin-secreting structures similar to pancreatic islets. *Science*. 2001;**292**:1389-1394

[20] Baskin DG, Erlandsen SL, Parsons JA. Immunocytochemistry with osmium-feed tissue. 1. Light microscopic localization of growth hormone and prolactin with the unlabeled antibody-enzyme method. *The Journal of Histochemistry and Cytochemistry*. 1979;**27**:867-872

[21] Bendayan M, Zollinger M. Ultrastructural localization of antigenic sites on osmium-fixed tissues applying the protein A-gold technique. *The Journal of Histochemistry and Cytochemistry*. 1983;**31**:101-109

[22] Nakai Y, Iwashita T. Correlative light and electron microscopy of the frog adrenal gland cells using adjacent Epon-embedded sections. *Archivum Histologicum Japonicum*. 1976;**39**:183-191

[23] Lacy PE. Electron microscopic identification of different cell types in the islets of Langerhans of the guinea pig, rat, rabbit and dog. *The Anatomical Record*. 1957;**128**:255-267

[24] Watari N, Tsukagoshi N, Honma Y. Correlative light and electron microscopy of the islets of Langerhans in some lower vertebrates.

Archivum Histologicum Japonicum. 1970;**31**:371-392

[25] Albers J, Pacilé S, Markus MA, Wiart M, Vande Velde G, Tromba G, et al. X-ray-based 3D virtual histology-adding the next dimension to histological analysis. *Molecular Imaging and Biology*. 2018;**20**:731-741. DOI: 10.1007/s11307-018-1246-3

[26] Begemann I, Galic M. Correlative light electron microscopy: Connecting synaptic structure and function. *Frontiers in Synaptic Neuroscience*. 2016;**8**:28. DOI: 10.3389/fnsyn.2016.00028

[27] Caplan J, Niethammer M, Taylor RM 2nd, Czymmek KJ. The power of correlative microscopy: Multi-modal, multi-scale, multi-dimensional. *Current Opinion in Structural Biology*. 2011;**21**:686-693

[28] Cortese K, Vicidomini G, Gagliani MC, Boccacci P, Diaspro A, Tacchetti C. High data output method for 3-D correlative light-electron microscopy using ultrathin cryosections. *Methods in Molecular Biology*. 2013;**950**:417-437

[29] Van Rijnsoever C, Oorschot V, Klumperman J. Correlative light-electron microscopy (CLEM) combining live-cell imaging and immunolabeling of ultrathin cryosections. *Nature Methods*. 2008;**5**:973-980

[30] Yin W, Mendenhall JM, Monita M, Gore AC. Three-dimensional properties of GnRH neuroterminals in the median eminence of young and old rats. *The Journal of Comparative Neurology*. 2009;**517**:284-295

[31] Wolff G, Hagen C, Grünwald K, Kaufmann R. Towards correlative super-resolution fluorescence and electron cryo-microscopy. *Biology of the Cell*. 2016;**108**:245-258

[32] Gibson KH, Vorkel D, Meissner J, Verbavatz JM. Fluorescing the electron:

Strategies in correlative experimental design. *Methods in Cell Biology*. 2014;**124**:23-54

[33] Huang B, Wang W, Bates M, Zhuang X. Three-dimensional super-resolution imaging by stochastic optical reconstruction microscopy. *Science*. 2008;**319**:810-813

[34] Hughes LC, Archer CW, ap Gwynn I. The ultrastructure of mouse articular cartilage: Collagen orientation and implications for tissue functionality. A polarised light and scanning electron microscope study and review. *European Cells & Materials*. 2005;**9**:68-84

[35] Jin SE, Bae JW, Hong S. Multiscale observation of biological interactions of nanocarriers: From nano to macro. *Microscopy Research and Technique*. 2010;**73**:813-823

[36] Robinson JM, Takizawa T, Pombo A, Cook PR. Correlative fluorescence and electron microscopy on ultrathin cryosections: Bridging the resolution gap. *The Journal of Histochemistry and Cytochemistry*. 2001;**49**:803-808

[37] Fox CH, Johnson FB, Whiting J, Roller PP. Formaldehyde fixation. *The Journal of Histochemistry and Cytochemistry*. 1985;**33**:845-853

[38] Saitoh S, Terada N, Ohno N, Ohno S. Distribution of immunoglobulin-producing cells in immunized mouse spleens revealed with “in vivo cryotechnique”. *Journal of Immunological Methods*. 2008;**331**:114-126

[39] Saitoh S, Terada N, Ohno N, Saitoh Y, Soleimani M, Ohno S. Immunolocalization of phospho-Arg-directed protein kinase-substrate in hypoxic kidneys using in vivo cryotechnique. *Medical Molecular Morphology*. 2009;**42**:24-31

[40] Cortese K, Diaspro A, Tacchetti C. Advanced correlative light/electron

microscopy: Current methods and new developments using Tokuyasu cryosections. *The Journal of Histochemistry and Cytochemistry*. 2009;**57**:1103-1112

[41] Oorschot VM, Sztal TE, Bryson-Richardson RJ, Ramm G. Immuno correlative light and electron microscopy on Tokuyasu cryosections. *Methods in Cell Biology*. 2014;**124**:241-258

[42] Nakane PK. States of the art of immunoelectron microscopy in Japan. *Journal of Electron Microscopy*. 1989;**38**(Suppl):S135-S141

[43] Oliver C. Pre-embedding labeling methods. *Methods in Molecular Biology*. 2010;**588**:381-386

[44] Orci L, Malaisse-Lagae F, Amherdt M, Ravazzola M, Weisswange A, Dobbs R, et al. Cell contacts in human islets of Langerhans. *The Journal of Clinical Endocrinology and Metabolism*. 1975;**41**:841-844

[45] Shimo S, Saitoh S, Saitoh Y, Ohno N, Ohno S. Morphological and immunohistochemical analyses of soluble proteins in mucous membranes of living mouse intestines by cryotechniques. *Microscopy (Oxford)*. 2015;**64**:189-203

[46] Tokuyasu KT. A study of positive staining of ultrathin frozen sections. *Journal of Ultrastructure Research*. 1978;**63**:287-307

[47] Tokuyasu KT, Singer SJ. Improved procedure for immunoferritin labeling of ultrathin frozen sections. *The Journal of Cell Biology*. 1976;**71**:891-906

[48] Shi SR, Cote RJ, Taylor CR. Antigen retrieval techniques: Current perspectives. *The Journal of Histochemistry and Cytochemistry*. 2001;**49**:931-937

- [49] Cattoretto G, Pileri S, Parravicini C, Becker MH, Poggi S, Bifulco C, et al. Antigen unmasking on formalin-fixed, paraffin-embedded tissue sections. *The Journal of Pathology*. 1993;**171**:83-98
- [50] Ohno S, Terada N, Ohno N, Saitoh S, Saitoh Y, Fujii Y. Significance of 'in vivo cryotechnique' for morphofunctional analyses of living animal organs. *Journal of Electron Microscopy*. 2010;**59**:395-408
- [51] O'Leary TJ, Mason JT. A molecular mechanism of formalin fixation and antigen retrieval. *American Journal of Clinical Pathology*. 2004;**122**:154; author reply 154-155
- [52] Parajuli LK, Fukazawa Y, Watanabe M, Shigemoto R. Subcellular distribution of $\alpha 1G$ subunit of T-type calcium channel in the mouse dorsal lateral geniculate nucleus. *The Journal of Comparative Neurology*. 2010;**518**:4362-4374
- [53] Shi SR, Key ME, Kalra KL. Antigen retrieval in formalin-fixed, paraffin-embedded tissues: An enhancement method for immunohistochemical staining based on microwave oven heating of tissue sections. *The Journal of Histochemistry and Cytochemistry*. 1991;**39**:741-748
- [54] Emoto K, Yamashita S, Okada Y. Mechanisms of heat-induced antigen retrieval: Does pH or ionic strength of the solution play a role for refolding antigens? *The Journal of Histochemistry and Cytochemistry*. 2005;**53**:1311-1321
- [55] Yamashita S. Heat-induced antigen retrieval: Mechanisms and application to histochemistry. *Progress in Histochemistry and Cytochemistry*. 2007;**41**:141-200
- [56] Yamashita S, Okada Y. Heat-induced antigen retrieval in conventionally processed Epon-embedded specimens: Procedures and mechanisms. *The Journal of Histochemistry and Cytochemistry*. 2014;**62**:584-597
- [57] Martell JD, Deerinck TJ, Sancak Y, Poulos TL, Mootha VK, Sosinsky GE, et al. Engineered ascorbate peroxidase as a genetically encoded reporter for electron microscopy. *Nature Biotechnology*. 2012;**30**:1143-1148
- [58] Lam SS, Martell JD, Kamer KJ, Deerinck TJ, Ellisman MH, Mootha VK, et al. Directed evolution of APEX2 for electron microscopy and proximity labeling. *Nature Methods*. 2015;**12**:51-54
- [59] Ou HD. Visualizing viral protein structures in cells using genetic probes for correlated light and electron microscopy. *Methods*. 2015;**90**:39-48
- [60] Shu X, Lev-Ram V, Deerinck TJ, Qi Y, Ramko EB, Davidson MW, et al. A genetically encoded tag for correlated light and electron microscopy of intact cells, tissues, and organisms. *PLoS Biology*. 2011;**9**:e1001041
- [61] Sonomura T, Furuta T, Nakatani I, Yamamoto Y, Unzai T, Matsuda W, et al. Correlative analysis of immunoreactivity in confocal laser-scanning microscopy and scanning electron microscopy with focused ion beam milling. *Frontiers in Neural Circuits*. 2013;**7**:1-7
- [62] Tsang TK, Bushong EA, Boassa D, Hu J, Romoli B, Phan S, et al. High-quality ultrastructural preservation using cryofixation for 3D electron microscopy of genetically labeled tissues. *eLife*. 2018. DOI: 10.7554/eLife.35524
- [63] Qi YB, Garren EJ, Shu X, Tsien RY, Jin Y. Photo-inducible cell ablation in *Caenorhabditis elegans* using the genetically encoded singlet oxygen generating protein miniSOG. *Proceedings of the National Academy of Sciences of the United States of America*. 2012;**109**:7499-7504

- [64] Onouchi T, Shiogama K, Mizutani Y, Takaki T, Tsutsumi Y. Visualization of neutrophil extracellular traps and fibrin meshwork in human fibrinopurulent inflammatory lesions: III. Correlative light and electron microscopic study. *Acta Histochemica et Cytochemica*. 2016;**49**:141-147
- [65] Sawaguchi A, Kamimura T, Yamashita A, Takahashi N, Ichikawa K, Aoyama F, et al. Informative three-dimensional survey of cell/tissue architectures in thick paraffin sections by simple low-vacuum scanning electron microscopy. *Scientific Reports*. 2018;**8**:7479. DOI: 10.1038/s41598-018-25840-8
- [66] Maxwell MH. Two rapid and simple methods used for the removal of resins from 1.0 micron thick epoxy sections. *Journal of Microscopy*. 1978;**112**:253-255
- [67] Ozawa H, Picart R, Barret A, Tougaard C. Heterogeneity in the pattern of distribution of the specific hormonal product and secretogranins within the secretory granules of rat prolactin cells. *The Journal of Histochemistry and Cytochemistry*. 1994;**42**:1097-1107
- [68] Haraguchi CM, Yokota S. Immunofluorescence technique for 100-nm-thick semithin sections of Epon-embedded tissues. *Histochemistry and Cell Biology*. 2002;**117**:81-85
- [69] D'Amico F, Skarmoutsou E, Stivala F. State of the art in antigen retrieval for immunohistochemistry. *Journal of Immunological Methods*. 2009;**341**:1-18
- [70] Matsui T, Onouchi T, Shiogama K, Mizutani Y, Inada K, Fuxun Y, et al. Coated glass slides TACAS are applicable to heat-assisted immunostaining and in situ hybridization at the electron microscopy level. *Acta Histochemica et Cytochemica*. 2015;**48**:153-157
- [71] Zhai XY, Kristoffersen IB, Christensen EI. Immunocytochemistry of renal membrane proteins on epoxy sections. *Kidney International*. 2007;**72**:731-735
- [72] Ye L, Robertson MA, Hesselson D, Stainier DY, Anderson RM. Glucagon is essential for alpha cell transdifferentiation and beta cell neogenesis. *Development*. 2015;**142**:1407-1417
- [73] Mojsov S, Heinrich G, Wilson IB, Ravazzola M, Orci L, Habener JF. Preproglucagon gene expression in pancreas and intestine diversifies at the level of post-translational processing. *The Journal of Biological Chemistry*. 1986;**261**:11880-11889
- [74] Ravazzola M, Perrelet A, Unger RH, Orci L. Immunocytochemical characterization of secretory granule maturation in pancreatic A-cells. *Endocrinology*. 1984;**114**:481-485
- [75] Varndell IM, Bishop AE, Sikri KL, Uttenthal LO, Bloom SR, Polak JM. Localization of glucagon-like peptide (GLP) immunoreactants in human gut and pancreas using light and electron microscopic immunocytochemistry. *The Journal of Histochemistry and Cytochemistry*. 1985;**33**:1080-1086
- [76] Pelletier G. Identification of four cell types in the human endocrine pancreas by immunoelectron microscopy. *Diabetes*. 1977;**26**:749-756
- [77] Braun M. The somatostatin receptor in human pancreatic b-cells. *Vitamins and Hormones*. 2014;**95**:165-193
- [78] Cnop M, Hughes SJ, Igoillo-Esteve M, Hoppa MB, Sayyed F, Van de Laar L, et al. The long lifespan and low turnover of human islet beta cells estimated by mathematical modelling of lipofuscin accumulation. *Diabetologia*. 2010;**53**:321-330
- [79] Borrett S, Hughes L. Reporting methods for processing and analysis of data from serial block face scanning

electron microscopy. *Journal of Microscopy*. 2016;**263**:3-9

[80] Denk W, Horstmann H. Serial block-face scanning electron microscopy to reconstruct three-dimensional tissue nanostructure. *PLoS Biology*. 2004;**2**:e329

[81] Heymann JAH, Gestmann M, Giannuzzi I, Lich LA, Subramaniam B. Site-specific 3D imaging of cells and tissues with a dual beam microscope. *Journal of Structural Biology*. 2006;**155**:63-73

[82] Kubota Y. New developments in electron microscopy for serial image acquisition of neuronal profiles. *Microscopy (Oxford)*. 2015;**64**:27-36

[83] Kubota Y, Sohn J, Hatada S, Schurr M, Straehle J, Gour A, et al. A carbon nanotube tape for serial-section electron microscopy of brain ultrastructure. *Nature Communications*. 2018;**9**:437. DOI: 10.1038/s41467-017-02768-7

[84] Micheva KD, Smith SJ. Array tomography: A new tool for imaging the molecular architecture and ultrastructure of neural circuits. *Neuron*. 2007;**55**:25-36

[85] Peddie CJ, Collinson LM. Exploring the third dimension: Volume electron microscopy comes of age. *Micron*. 2014;**61**:9-19

[86] Ohno N, Katoh M, Saitoh Y, Saitoh S, Ohno S. Three-dimensional volume imaging with electron microscopy toward connectome. *Microscopy (Oxford)*. 2015;**64**:17-26

[87] Pfeifer CR, Shomorony A, Aronova MA, Zhang G, Cai T, Xu H, et al. Quantitative analysis of mouse pancreatic islet architecture by serial block-face SEM. *Journal of Structural Biology*. 2015;**189**:44-52

[88] Nguyen HB, Thai TQ, Saitoh S, Wu B, Saitoh Y, Shimo S, et al. Conductive

resins improve charging and resolution of acquired images in electron microscopic volume imaging. *Scientific Reports*. 2016;**6**:23721

[89] Ben-Othman N, Vieira A, Courtney M, Record F, Gjernes E, Avolio F, et al. Long-term GABA administration induces alpha cell-mediated beta-like cell neogenesis. *Cell*. 2017;**168**:73-85

[90] Bruneval P, Hinglais N, Alhenc-Gelas F, Tricottet V, Corvol P, Menard J, et al. Angiotensin I converting enzyme in human intestine and kidney. Ultrastructural immunohistochemical localization. *Histochemistry*. 1986;**85**:73-80

[91] Buffa R, Polak JM, Pearse AG, Solcia E, Grimelius L, Capella C. Identification of the intestinal cell storing gastric inhibitory peptide. *Histochemistry*. 1975;**43**:249-255

[92] Jonsson A, Ladenvall C, Ahluwalia TS, Kravic J, Krus U, Taneera J, et al. Effects of common genetic variants associated with type 2 diabetes and glycemic traits on α - and β -cell function and insulin action in humans. *Diabetes*. 2013;**62**:2978-2983

[93] Klöppel G, Lenzen S. Anatomy and physiology of the endocrine pancreas. In: Klöppel G, Heitz PU, editors. *Pancreatic Pathology*. London: Churchill Livingstone; 1984. pp. 133-153

[94] Suleiman H, Zhang L, Roth R, Heuser JE, Miner JH, Shaw AS, et al. Nanoscale protein architecture of the kidney glomerular basement membrane. *eLife*. 2013;**2**:e01149

[95] Wu M, Huang B, Graham M, Raimondi A, Heuser JE, Zhuang X, et al. Coupling between clathrin-dependent endocytic budding and F-BAR-dependent tubulation in a cell-free system. *Nature Cell Biology*. 2010;**12**:902-908

[96] Koga D, Kusumi S, Ushiki T, Watanabe T. Integrative method for three-dimensional imaging of the entire Golgi apparatus by combining thiamine pyrophosphatase cytochemistry and array tomography using backscattered electron-mode scanning electron microscopy. *Biomedical Research*. 2017;**38**:285-296

[97] Makhijani K, To TL, Ruiz-González R, Lafaye C, Royant A, Shu X. Precision optogenetic tool for selective single- and multiple-cell ablation in a live animal model system. *Cell Chemical Biology*. 2017;**24**:110-119

[98] Rizzo R, Parashuraman S, Luini A. Correlative video-light-electron microscopy: Development, impact and perspectives. *Histochemistry and Cell Biology*. 2014;**142**:133-138

[99] Yamashita S, Katsumata O, Okada Y. Establishment of a standardized post-embedding method for immunoelectron microscopy by applying heatinduced antigen retrieval. *J Electron Microsc* (Tokyo). 2009;**58**:267-279